Climate Dynamics (2019) 53:1023–1037
https://doi.org/10.1007/s00382-019-04629-z

Tree rings reveal hydroclimatic fingerprints of the Pacific Decadal Oscillation on the Tibetan Plateau

Lixin Lyu[1,2] · Ulf Büntgen[2,3,4,5] · Kerstin Treydte[2] · Kailiang Yu[6] · Hanxue Liang[7] · Frederick Reinig[2] · Daniel Nievergelt[2] · Mai-He Li[2] · Paolo Cherubini[2]

Received: 12 August 2018 / Accepted: 10 January 2019 / Published online: 16 January 2019

Abstract
Predicting hydroclimatic changes on the Tibetan Plateau (TP) is crucial for managing water and ecosystems for the well-being of millions of people. Our understanding of the synoptic conditions on the TP is, however, still limited due to the paucity of meteorological measurements and proxy-based, high-resolution climate reconstructions. Here, we use state-of-the-art dendroclimatological techniques to investigate the paleoclimatic potential of drought-sensitive *Picea likiangensis* var. *balfouriana* forests between 4000 and 4500 m asl on the southeastern TP (SETP). The newly developed tree-ring width chronology correlates significantly with yearly changes in regional relative air humidity (RH) ($r = 0.85$, $P < 0.001$, 1978–2011). A new 407-year-long reconstruction of RH over the hydrological year from previous year August to July of the year of ring formation shows that, despite the generally humid conditions, four of the ten driest years are observed in the twentieth century with 1983 having been the driest. On the other hand, seven out of the ten most humid years were found in the eighteenth century. Our reconstruction reveals that the Pacific Decadal Oscillation (PDO) is the dominant climate driver at multi-decadal scales, but the relationships are not stable over time, with unknown underlying mechanisms. Although our study demonstrates the importance of the PDO for hydroclimate projections on the TP, caution is advised when considering only its most recent fluctuations.

Keywords Climate dynamics · Dendroclimatology · Drought extremes · Hydroclimate · Proxy reconstruction · Relative humidity · Tree rings

1 Introduction

Drought extremes, which are characterized by above-average seasonal or annual water deficits, have a wide range of ecological and economic consequences (Mishra and Singh 2010; Trnka et al. 2018). Increasing air temperatures will change the pace of the hydrological cycle as more water evaporates to the atmosphere. This may result in increased rainfall variability at different time scales (Yu et al. 2017) and lead dry regions to become drier and humid regions to become more humid (Chou et al. 2009). Such crucial changes, which are expected to accelerate in the future, significantly affect ecosystem services and functioning, as well

Electronic supplementary material The online version of this article (https://doi.org/10.1007/s00382-019-04629-z) contains supplementary material, which is available to authorized users.

✉ Lixin Lyu
lixinlv@ibcas.ac.cn

[1] State Key Laboratory of Vegetation and Environmental Change, Institute of Botany, Chinese Academy of Sciences, 20 Nanxincun, Haidian District, Beijing 100093, People's Republic of China

[2] Swiss Federal Research Institute WSL, Zürcherstrasse 111, 8903 Birmensdorf, Switzerland

[3] Department of Geography, University of Cambridge, Downing Place, Cambridge CB2 3EN, UK

[4] Global Change Research Centre (CzechGlobe), Bělidla 986/4a, 60300 Brno, Czech Republic

[5] Department of Geography, Faculty of Science, Masaryk University, Kotlářská 2, 613 00 Brno, Czech Republic

[6] Institute of Integrative Biology, ETH Zürich, Universitätstrasse 16, 8006 Zurich, Switzerland

[7] Key Laboratory of Vegetation Restoration and Management of Degraded Ecosystems, South China Botanical Garden, Chinese Academy of Sciences, 723 Xingke Road, Tianhe District, Guangzhou 510650, People's Republic of China

as hydrological, biogeochemical and ecological processes (Chen et al. 2018). Predicting how hydroclimate will change in a region therefore plays a major role in water resources management and the assessment of drought or flood risks, and has important implications for human communities (Bordi and Sutera 2007). This effort, however, remains a challenge because of the interplay of multiple synoptic climatic drivers and because of the paucity of climate records in both space and time.

The Tibetan Plateau (TP), also known as the "Water Tower of Asia", harbours the snow and ice that feed the headwaters of Asia's major rivers (Xu et al. 2008). Forecasting future hydroclimate changes on the TP is therefore critical to the wellbeing of billions of people in Asia. The TP has experienced significant warming over the past decades (Duan et al. 2015; Liu et al. 2017), which we now know to be unprecedented in at least the past six centuries (Liang et al. 2009; Zhu et al. 2011). Consequently, severe permafrost melting (Wu and Zhang 2010) and a remarkable shrinkage of glacial areas (Yao et al. 2012) have been reported. Nonetheless, our knowledge regarding hydroclimate variability on the TP is still limited and controversial. Some studies suggest that the severity and spatial extent of drought stress has been increasing (Ding et al. 2018; You et al. 2015) due to the exponential response of saturated vapour pressure to increasing air temperature (Eamus et al. 2013; Seager et al. 2015). Increases in precipitation have not been sufficiently significant to counterbalance this trend (Wan et al. 2017). In contrast, other studies report a trend towards overall more humid conditions (Lamsal et al. 2017; Zhang et al. 2017a), which are more favourable for vegetation.

Hydroclimate variability on the Tibetan Plateau is particularly high because of the complex interplay of different synoptic drivers (Fig. 1), including the effects of the Indian (Webster et al. 1998) and East Asian monsoons (Morrill et al. 2003; Winkler and Wang 1993), the Atlantic Multidecadal Oscillation (AMO) (Krishnamurthy and Krishnamurthy 2016; Liang et al. 2016), and other common external climatic forcing factors such as solar (Duan and Zhang 2014; Wang and Zhang 2011) and volcanic activity (Anchukaitis et al. 2010). Indeed, because of the complex mountain structure and orography of the TP, which strongly influence local circulation, different determinant drivers affect hydroclimate variability at the local level in different regions of the TP.

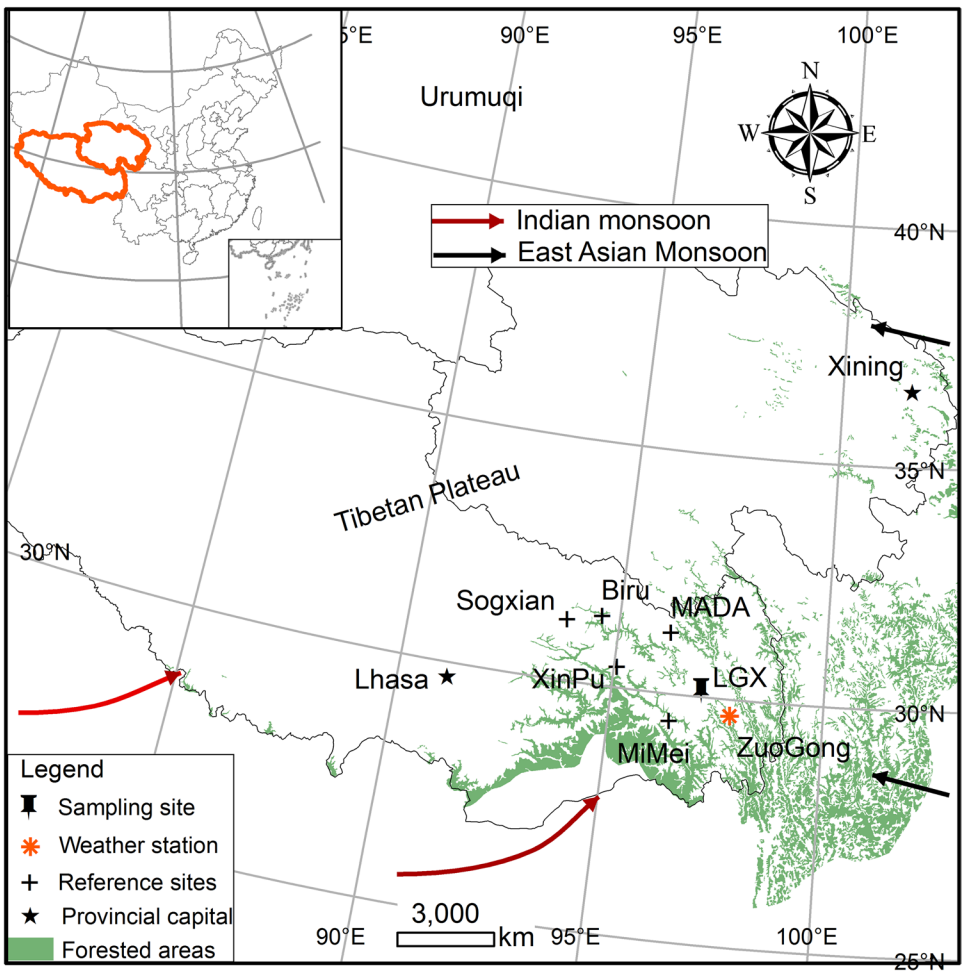

Fig. 1 Location of the study site on the southeastern Tibetan Plateau

For instance, a north–south dipole of moisture conditions was observed in the reconstruction of a meridional moisture stress gradient index based on a network of 23 moisture-sensitive tree-ring width chronologies on the eastern TP (Zhang et al. 2015). To disentangle the influences of different synoptic drivers and to gain a deeper understanding of the mechanisms regulating the hydroclimate variations on the TP, more high-resolution paleoclimatic data are needed (Chou et al. 2009; Seager and Vecchi 2010).

Numerous efforts have been undertaken to reconstruct past climate variability on the TP, including air temperature (Bräuning and Mantwill 2004; Gou et al. 2014; He et al. 2014; Liu et al. 2009), precipitation (Cai et al. 2015; Grießinger et al. 2011; Sheppard et al. 2004), and soil moisture indices such as the Palmer Drought Severity Index (PDSI) (Fan et al. 2008; Fang et al. 2009; Wang et al. 2008) and the Standardized Precipitation Evapotranspiration Index (SPEI) (Nie et al. 2017). Climate variables representing atmospheric drought conditions such as relative humidity (RH), however, have received less attention (You et al. 2015). Representing a key component of a region's hydroclimate, atmospheric drought is different from soil drought, and affects tree physiological processes (Saurer et al. 2000) and forest productivity (Novick et al. 2016). Understanding past variability in atmospheric moisture is thus essential for reducing uncertainties in projections of climate and ecosystem dynamics.

Only a handful of air humidity reconstructions are available for the TP. According to a summer RH reconstruction based on tree-ring cellulose $\delta^{18}O$, a distinct drying trend is apparent on the eastern TP since the 1870s (Wernicke et al. 2015). Subsequently, Wernicke et al. (2017) presented two moisture-sensitive tree-ring $\delta^{18}O$ chronologies for the southeastern Tibetan Plateau (SETP) that show a humid period during 1700–1850 CE and a drying trend since the mid-nineteenth century. Similarly, a tree-ring $\delta^{18}O$-based reconstruction by Grießinger et al. (2017) confirms a recent drying trend on the TP but shows that such a trend is not unprecedented in regard to the last 1500 years. Conversely, a RH reconstruction for the period 1751–2005 showed no significant centennial trend on the SETP from the 1820s through the 2000s, despite a weakening of the Asian summer monsoon and climatic warming during the 1980s–2000s (Shi et al. 2018). The disagreement between the few existing RH reconstructions for the TP calls for the development of additional reconstructions of atmospheric drought variability to deepen our understanding of its underlying synoptic drivers.

Here, we investigate an old-growth *Picea likiangensis* var. *balfouriana* (Rehder & E.H. Wilson) Hillier forest on the SETP, where hydroclimate variations are potentially regulated by branches of both the Indian and the East Asian Monsoon systems (Fig. 1). We develop a 407-year-long RH reconstruction and study its teleconnection to the major synoptic drivers with the goal of identifying the main synoptic climatic circulation patterns that control hydroclimate variability in this region.

2 Materials and methods

2.1 Study area and tree-ring sampling

The study area is located in Basu County of the SETP, where climate is mainly affected by the Asian Summer Monsoon system and where temperature and precipitation maxima typically occur during the summer months (Fig. 1). We used climate data from the Zuogong weather station (29°40′N, 97°50′E, 3780 m asl) for the period between 1978 and 2011. Mean annual temperature over this period was 4.7 °C. Annual precipitation was 450 mm, with about 82% of the precipitation falling during the monsoon season (from June to September) (Fig. 2). The study species is *P. likiangensis* var. *balfouriana* (Rehder & EH Wilson) Hillier, which is a frost- and drought-tolerant coniferous species growing on the shady or semi-shady slopes of mountains, where it usually forms a pure forest.

During summer 2012, we collected increment core samples from trees at three elevations spanning from the lowest forest distribution limit at around 4017 m asl to the upper treeline at around 4495 m asl (Fig. 1; Table 1). At the treeline, we set up three rectangular plots perpendicular to the timberline (the upper limit of the forest border with at least 20% canopy coverage), 30 meters in width and 100 to

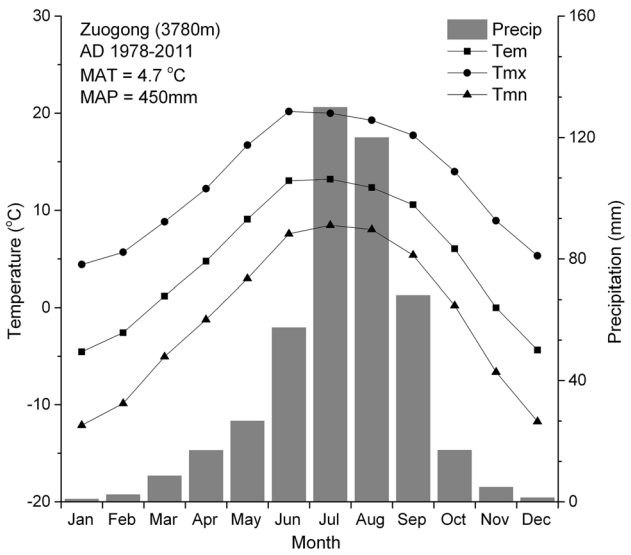

Fig. 2 Climate diagram for the Zuogong weather station (3780 m) for the period 1978–2011. *MAT* mean annual temperature, *MAP* mean annual precipitation. *Tem* monthly mean temperature, *Tmx* monthly mean maximum temperature, *Tmn* monthly mean minimum temperature, *Precip* mean monthly precipitation sum

Table 1 Site information and statistical metrics of the tree-ring width measurements

Site	Lon	Lat	Alt	Span	Trees	MSL	MTRW	SD	Skew	MS	Gini	AR1
Upper	97.111	30.129	4495	1377	61	275	0.67	0.31	0.90	0.25	0.27	0.74
Middle	97.112	30.133	4250	1583	19	283	0.59	0.28	0.77	0.22	0.26	0.79
Lower	97.114	30.136	4017	1592	22	238	0.43	0.23	0.87	0.38	0.30	0.55
Composite	–	–	–	1377	102	275	0.67	0.31	0.90	0.25	0.27	0.74

Span the longest time span of the oldest tree, *Trees* number of sampled trees/cores (one core per tree), *MSL* mean segment length, *MTRW* mean tree-ring width, *SD* standard deviation, *Skew* asymmetry of data distribution, *MS* mean sensitivity, *Gini* Gini coefficient, *AR1* first-order autocorrelation

180 meters in length depending on the distribution of trees above the timberline. All trees larger than 5 cm in diameter at breast height were cored. Since enough number of old trees could be accessed in a relatively short distance at the middle and lower elevations, we took cores from the 30 largest-diameter trees without setting up plots.

2.2 Development of the tree-ring width chronology

In the laboratory, the increment cores were air-dried, mounted on wooden holders, and polished with progressively finer sandpaper until ring boundaries were clearly visible. Tree rings were visually examined and cross-dated with a stereomicroscope (Leica Microsystems, Germany) by comparing the ring patterns among samples. The ring widths of each sample were then measured to a resolution of 0.001 mm using the Lintab-5 System (Lintab, Germany) and then quality-checked and cross-dated using the COFECHA program (Holmes 1983). To preserve long-term signals in the tree-ring records and to avoid potential age-related biases in the response to climate, only tree cores with cross-dated ages of at least 100 years were retained for further analysis.

In order to get rid of age- and size-related growth trends while preserving any climate-related variations, a cubic smoothing spline with a 50% frequency–response cut-off at the 200-year length was used to fit each raw tree-ring width series. A tree-ring index series of each sample was subsequently obtained by calculating ratios of the ring-width measurements and the fitted splines per year. All tree-ring index series were then averaged to obtain three elevational site chronologies by computing the bi-weight robust mean in order to reduce the influence of outliers (Cook and Kairiukstis 1990). To check the coherence between the three site chronologies, running correlations were calculated using a window of 50-year length with 25-year overlap over the entire common period. Given the strong common variations, we developed a single composite tree-ring width chronology from all of the tree-ring series using the same method as for the site chronologies (Fig. S1).

Standard dendrochronological descriptive statistics were calculated to assess the quality of the standardized chronology. Mean sensitivity (MS) is an indicator of the relative change in ring widths between consecutive years; a higher MS suggests more sensitivity of tree-ring growth to interannual environmental changes. The Gini coefficient (Gini) measures the inequality among values of a frequency distribution, summarizing data heterogeneity with a single number. Higher values indicate higher diversity (Biondi and Qeadan 2008). The first-order autocorrelation (AC1) assesses the relationship between growth in 1 year relative to the previous year. Common signal strength was evaluated using mean inter-series correlation (R_{bar}) and the percent variance explained by the first principal component (PC1). The Expressed Population Signal (EPS) and signal-to-noise ratio (SNR) are functions of correlation (r) and sample size, and evaluate the signal strength of the chronology. PC1 and SNR were calculated for the common period 1851–2000 CE. The median segment length (MSL) is a useful diagnostic for determining the maximum low-frequency signal resolvable in a tree-ring chronology (see Cook and Kairiukstis 1990, pages 137–153). The Expressed Population Signal (EPS) indicates the point at which replication within the chronology is high enough to ensure reliability; an EPS value > 0.85 indicates chronology reliability (Wigley et al. 1984).

2.3 Growth-climate relationships

In order to decipher the climate signals embedded in tree growth variations, we calculated the Pearson Product-Moment Correlation coefficients (r) between tree-ring indices and climate variables for the period 1978–2011. Because the climate conditions of the previous year may affect tree-ring growth in the current year (Fritts 1976), correlations between the tree-ring width chronologies and monthly climate variables were calculated from previous May to current September. The climate variables include monthly mean temperature, monthly total precipitation, and monthly mean relative humidity measured at the Zuogong weather station (Fig. 2). In order to better represent the water availability conditions, we calculated potential evapotranspiration (PET) using Thornthwaite's empirical method (Kumar et al. 1987), and reference evapotranspiration (ET_0) using the FAO Penman–Monteith method, which explicitly incorporates both physiological and aerodynamic parameters (Allen et al.

1998). The Standardized Precipitation Evapotranspiration Index (SPEI), another commonly used drought index, was also calculated based on climate records from the Zuogong weather station using the R package SPEI (Beguería and Vicente-Serrano 2017). All calculations and significance testing were processed using the R software (R Core Team 2018).

Due to the short time span of climate records from the nearest climate station (starting in 1978), we also correlated the composite tree-ring width chronology with climate variables from CRU TS4.01 spatially gridded climate data (https://crudata.uea.ac.uk/cru/data/hrg/cru_ts_4.01/) (Harris et al. 2014) obtained from the KNMI Climate Explorer (http://climexp.knmi.nl). Although the CRU data cover the period 1901–2016, most of the instrumental records in our study region do not predate the 1950s. We therefore focused only on the period 1950–2011.

2.4 Calibration/validation tests

The climate variable with the highest correlation with the composite chronology was reconstructed over the full length of the chronology. A linear regression was used to develop a transfer function with the tree-ring chronology as the independent variable and the climate data as the dependent variable. To validate the linear model, a cross-validation method (Michaelsen 1987) was used. The verification statistics calculated over multiple leave-one-out regressions include: Pearson's correlation (r), explained variance (R^2), adjusted explained variance (R^2_{adj}), root mean square error (RMSE), reduction of error (RE), sign test (ST), and product means test (PMT) (see Cook and Kairiukstis 1990, pages 178–185).

2.5 Regime shift tests of the climate reconstruction

To characterize the temporal variation of the climate reconstruction, regime shift analysis was conducted using the Shift Detection Program version 3.2 (http://www.beringclimate.noaa.gov/regimes/). The algorithm for the program is based on sequential t-tests that can detect the possibility of a regime shift in mean values through time (Rodionov 2004). The sliding window for calculating the t-tests was set at 10 years with a significance level of $P < 0.05$. The climate states and abrupt changes were compared with the pattern of climate changes reported in other studies around the region.

2.6 Spectral coherence analyses

Pacific Decadal Oscillation (PDO) is the leading principle component of monthly sea surface temperature (SST) anomalies in the North Pacific Ocean poleward of latitude 20°N (Zhang et al. 1997). In this study, we performed a spectral analysis using a multi-taper method (MTM) (Thomson 1982) to decompose the series and explore the relationship between the RH_{87} reconstruction and the Pacific Decadal Oscillation (PDO) over the common period. In particular, we examined the spectral coherency characteristics and identified the peak response band of the association between the two series at muti-decadal scales. The monthly PDO series were generated based on UKMO Historical SST and Reynold's Optimally Interpolated SST datasets. The data are publicly available at http://research.jisao.washington.edu/pdo/PDO.latest.

3 Results

3.1 Tree-ring width chronology

Mean tree-ring width increased from 0.43 mm at the lower site to 0.67 mm at the upper treeline with increasing standard deviation. High sensitivity of tree radial growth to environmental variations was indicated by reasonably high values of mean sensitivity (ranging from 0.22 to 0.38) and Gini coefficients (ranging from 0.26 to 0.30) (Table 1). A total of 102 crossdated cores from the upper treeline and two lower elevations sites were used in this study (Table 1). MSL ranges from 238 at the lowest site to 283 at the middle site, with an overall mean value of 275 for the composite chronology.

Consistently strong correlations among the three site chronologies were observed over the full length of the chronology (Fig. S1), indicating the suitability of these tree-ring series for the development of a robust composite chronology. As the number of samples decreased back in time, a well-replicated chronology period (1605–2011 CE) was selected on the basis of expressed population signal (EPS) being above 0.85. The 50-year moving Rbar for the composite chronology ranges from 0.31 to 0.54 (Fig. 3).

3.2 Relationship between tree-ring growth and climate

Relative humidity from previous year August to the current July of ring formation was the climate variable that correlated best with tree-ring growth ($r = 0.85$, $n = 33$, $P < 0.001$). The second best correlation was found to be total precipitation over the same season ($r = 0.65$, $n = 33$, $P < 0.001$), although no significant correlations were found for any individual month (Fig. 4). However, significant but clearly weaker correlations were found between tree growth and monthly temperatures of previous November and current February and April (Fig. 4). These climate-growth relationships were similar at each of the three elevational sites (Figs. S2–S4). Furthermore, we found significant but lower correlations between the composite chronology and drought indices including vapour pressure deficit (VPD) and

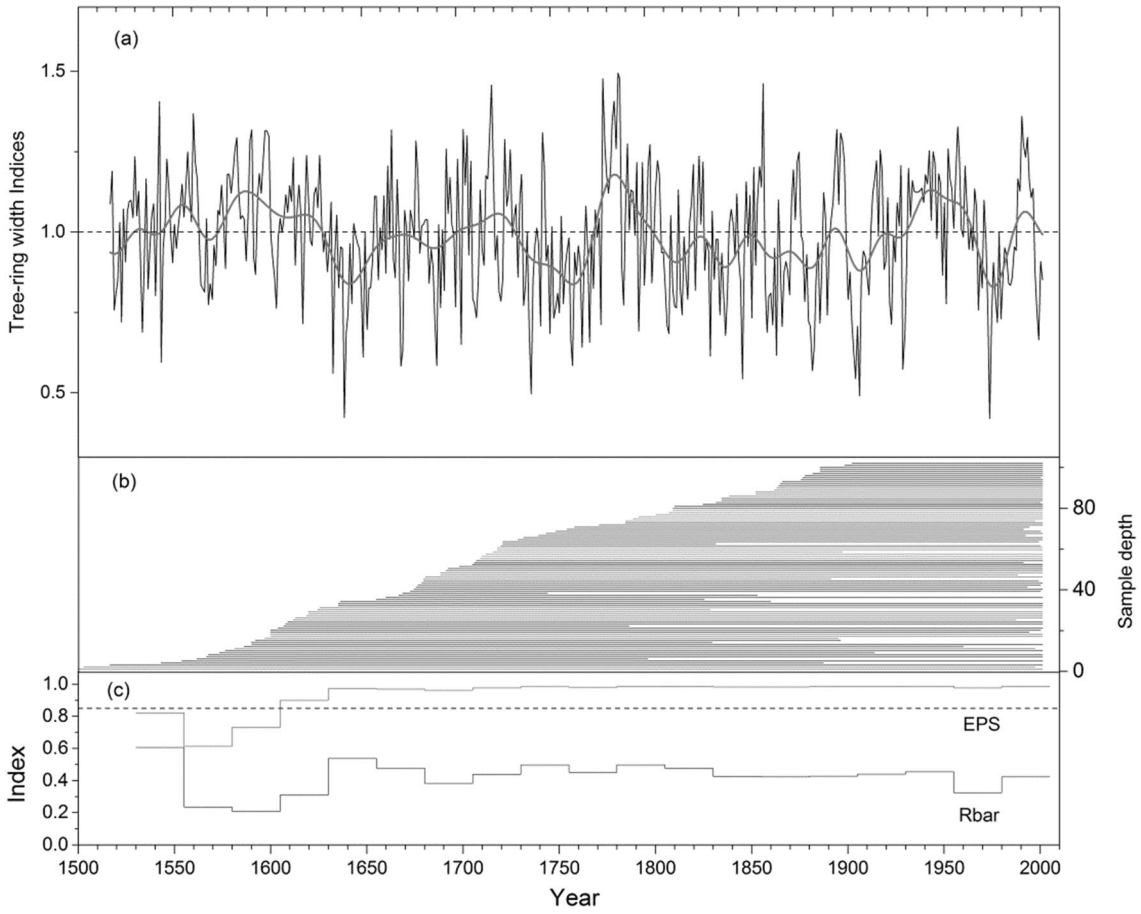

Fig. 3 Tree-ring width chronology for the site LGX, southeastern Tibetan Plateau. The bold red curve in **a** is a 20-year Sacizky-Golay filter (Savitzky and Golay 1964). The horizontal lines in **b** denote the spans of all tree-ring samples. The dotted line in **c** indicates the 0.85 expressed population signal (EPS) threshold, above which chronologies are considered reliable

Standardized Precipitation-Evapotranspiration Index (SPEI) during previous and current summer (Fig. S5).

The spatial extent of the climate-growth relationships was further examined by calculating correlation fields between tree-ring indices and spatially gridded CRU data. The correlation fields between the tree-ring width chronology and spatially gridded RH (Fig. S6) and precipitation (Fig. S7) show a correlation peak on the SETP. However, the correlations are lower than those with RH recorded at the weather station.

3.3 Reconstruction of mean relative humidity of the hydrologic year (RH_{87})

Based on the above growth-climate relationships, the mean RH of the hydrologic year (from previous August to current July of tree ring formation, RH_{87}) was reconstructed. The relative humidity data recorded at the Zuogong weather station were used to develop the transfer function over the period 1978–2011. The transfer function was a linear regression model of RH_{87} against the composite tree-ring width chronology as follows:

$$RH_{87} = 41 + 14.5 \times TRW \quad (1)$$

where *TRW* is the composite tree-ring width chronology. The final model accounted for 72% ($P < 0.001$) of the total variance in the RH_{87} over the calibration period 1979–2011 (Fig. 5b). In the leave-one-out cross validation, the values of r (0.83) and R^2 (0.69) are high and close to the values found in the calibration. The reduction of error (RE), sign test (ST), and product means test (PMT) are all significant at $P < 0.001$, with MSE being 3.75 and RMSE being 1.94 for the validation (Table 2). These statistics suggest that the calibration/regression model is strong and stable. The RH_{87} was reconstructed for the period 1605–2011 by applying the tree-ring data to the transfer function (Fig. 5a).

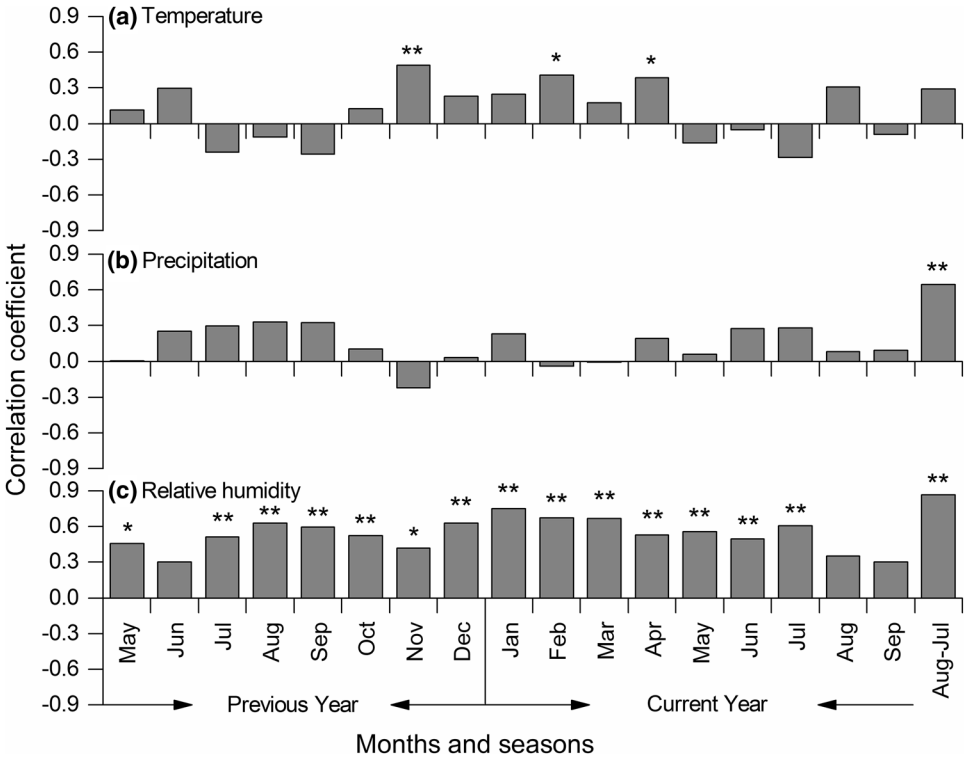

Fig. 4 Correlations of the tree-ring width chronology with climate variables for the period 1978–2011 as recorded at the Zuogong weather station. Aug-Jul indicates the seasonal average of the monthly data from previous August until current July of tree-ring formation. * and ** denote significance at levels of $P < 0.05$ and $P < 0.01$, respectively

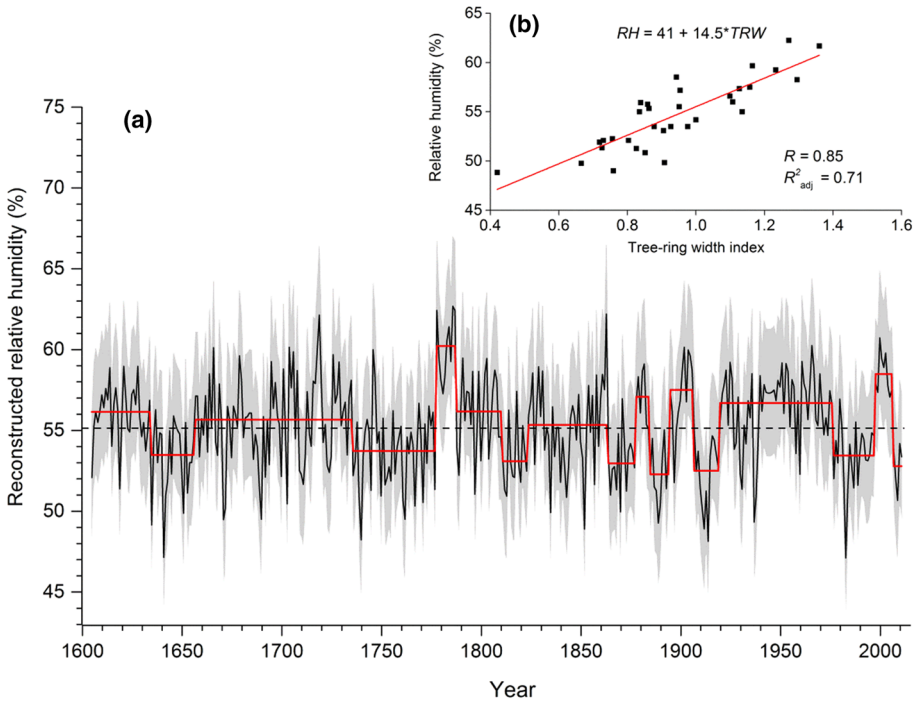

Fig. 5 Reconstructed mean relative humidity of the hydrological year (August–July) based on tree-ring widths from site LGX on the southeastern Tibetan Plateau (**a**) together with the corresponding transfer function (**b**). The red line indicates the regime of means for the relative humidity reconstruction, which was calculated using the sequential regime shift detection software *Shift detection v3-2* (Rodionov 2004)

3.4 Variations in the RH_{87} reconstruction

The shifting points identified in the regime shift analysis provided an objective criterion for detecting the warm/cold periods from the reconstructed RH_{87} history (Fig. 5b). Eight distinct drought episodes were identified: 1635–1656, 1736–1777, 1811–1823, 1864–1877, 1885–1894, 1907–1919, 1977–1997, and 2007–2011. Similarly, five noticeable long-lasting humid episodes were found in 1778–1787, 1878–1884, 1895–1906, 1920–1976,

Table 2 Calibration and verification statistics of the annual (previous August–July) mean relative humidity (RH_{87}) reconstruction model using the leave-one-out method for the period 1979–2011

Calibration				Validation						
r	R^2	R^2_{adj}	F	r	R^2	RE	MSE	RMSE	ST	PMT
0.85^{***}	0.72^{***}	0.71^{***}	79.96^{***}	0.83^{***}	0.69^{***}	0.69	3.75	1.94	26+/7- ***	4.09^{***}

The climate records are from the Zuogong station, southeastern Tibetan Plateau

r Pearson's correlation, R^2 variance explained, R^2_{adj} variance explained adjusted by degrees of freedom, *RE* reduction of error, *ST* prediction sign test

'+': pair of actual and predicted temperatures showing same sign of departure from their respective mean values; '−': different sign of departure; a non-parametric test is then performed based on the numbers of '+' and '−', PMT: t-value of product means test. $^{***}P<0.001$

Table 3 The ten driest and the ten most humid years over the past four centuries based on the hydraulic year mean relative humidity (RH_{87}) reconstruction

Rank	Driest years	Number of SDs from mean	Most humid years	Number of SDs from mean
1	1983	−2.85	1786	2.65
2	1641	−2.83	1778	2.56
3	1914	−2.48	1787	2.56
4	1740	−2.45	1863	2.48
5	1852	−2.22	1719	2.46
6	1912	−2.21	1784	2.20
7	1635	−2.12	2000	1.96
8	1889	−2.08	1783	1.88
9	1937	−2.06	1966	1.79
10	1671	−2.01	1704	1.75

and 1998–2006. According to the reconstruction, the most humid period occurred during the period 1778–1787. The twentieth century was also characterized by general above-average humidity, especially during the period 1998–2006, which was the second most humid episode in the past four centuries (Fig. 5b). In spite of the generally humid conditions, four of the ten driest years are observed in the twentieth century, with 1983 having been the driest. On the other hand, seven out of the ten most humid years were found in the eighteenth century (Table 3).

3.5 Correlations with PDO and global SST

A close association between PDO and the reconstructed relative humidity variations was detected, especially at decadal scales (Fig. 6). This teleconnection was further evidenced by the significant correlations between the instrumental records of relative humidity (Zuogong station) and the mid-western Pacific SSTs (Fig. S8). According to the spectral coherence analysis, our reconstructed RH_{87} was significantly correlated with the PDO reconstruction of MacDonald and Case (2005), peaking at a 39-year periodicity (Fig. 6b). This relationship, however, was not temporally stable throughout the common period since 1605 CE. A general antiphase relationship between the two series is observed over the past four centuries, except for a significant inphase epoch occurring in the first half of the eighteenth century (Fig. 6b, c). In the instrumental period of PDO, the inter-series correlation is weak before approximately 1950 ($r=0.08$, $P>0.05$), then becomes significant and negative during the period 1950–2000 ($r=-0.54$, $P<0.001$). After the beginning of the twenty-first century, a sharp reversal from a negative to a positive relationship is observed ($r=0.68$, $P<0.01$) (Fig. 6a).

To further test the association between PDO and our reconstructed hydroclimate record, we correlated the RH_{87} against HadlSST1 sea surface temperatures (SST) over the periods 1870–1950 (Fig. 7a) and 1951–2010 (Fig. 7b). We found continuous positive correlation fields in the tropical Pacific Ocean before 1950, but not over the equatorial areas (Fig. 7a). In the period 1951–2010, the significant correlation fields moved northward to the mid-western Pacific (around N30°). The correlation fields in the north Atlantic also strengthened during this period (Fig. 7b). Despite minor changes in the amplitudes, these northward shifts of the response centre from the tropical Pacific to the north-central Pacific were also observed in the correlations between reconstructed RH_{87} and SST from both ERSST V5 (Fig. S9) and ICOADS V2.5 (Fig. S10) datasets.

4 Discussion

4.1 Moisture-controlled tree-ring growth at high and low elevations

It is generally assumed that trees in high-elevation forests, especially at treelines, respond positively to vegetation-season air temperatures, as is observed in many extratropical treelines (Körner and Paulsen 2004; Kullman 2002; Smith et al. 2009). Such a response has been found at a number of treeline sites on the TP (Liang et al. 2009; Lv and Zhang

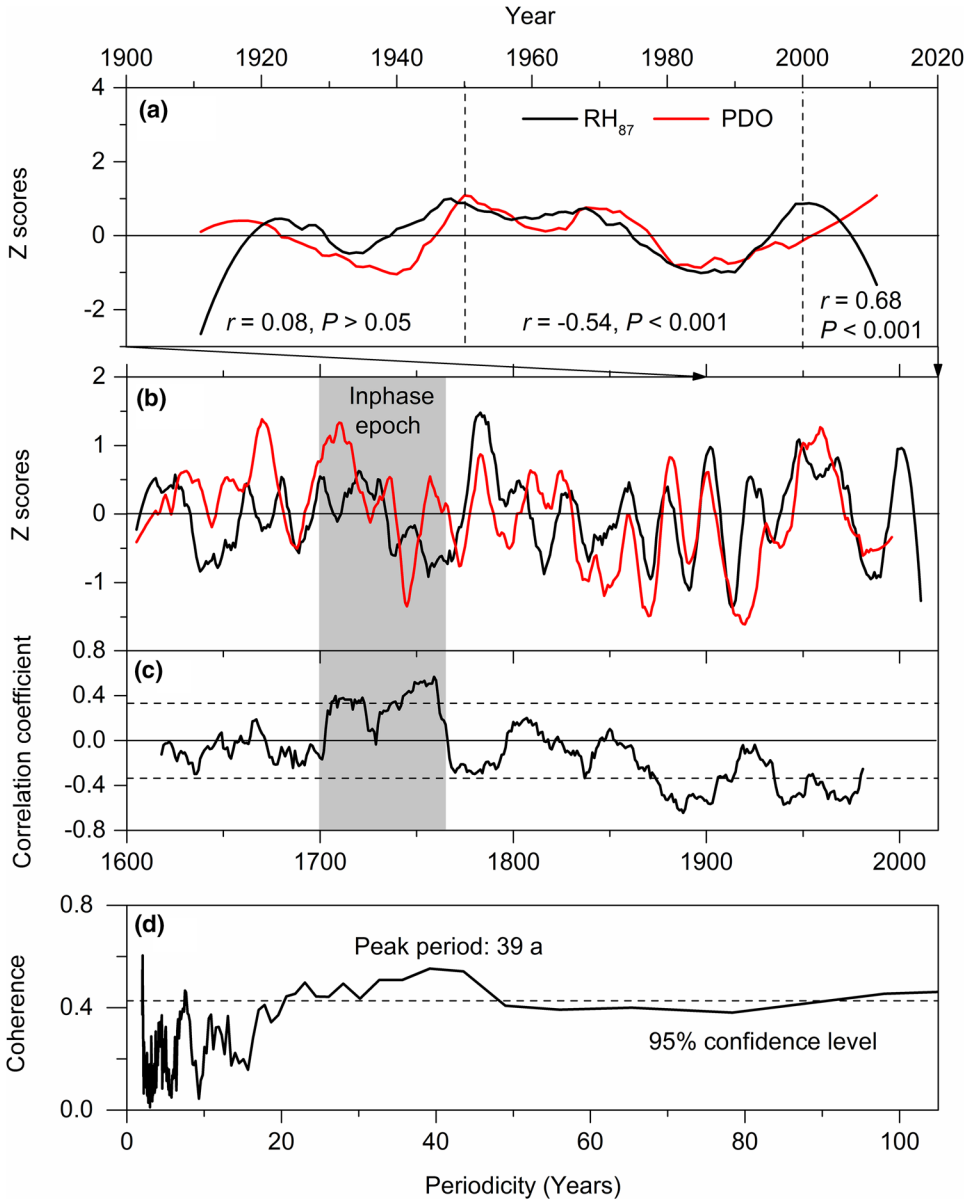

Fig. 6 Comparisons between the reconstructed relative humidity (RH_{87}) on the southeastern Tibetan Plateau and instrumental (**a**) or reconstructed (MacDonald and Case 2005) (**b**) Pacific Decadal Oscillation (PDO); the moving correlations between RH87 and the reconstructed PDO along a 30-year sliding window (**c**); and the coherence between RH_{87} and reconstructed PDO over the common period 1605–1996 using the multi-taper method (MTM) spectral analysis (**d**). Note that both the RH87 and PDO series were first centred to 0 and rescaled to a standard deviation of 1, and then smoothed using 20-year Sacizky-Golay filters (Savitzky and Golay 1964). The PDO series in **a** and **b** were multiplied by − 1 for clarity. The vertical broken lines in **a** separate the series into three periods; the correlation statistics are provided for each period. The horizontal broken lines in **c** and **d** denote a significance level of 0.05. The horizontal straight lines at 0 in (**a**–**c**) were superposed to facilitate interpretation of phase positions of the curves

2013; Zhu et al. 2011). In this study, however, we report a moisture-sensitive *P. likiangensis* var. *balfouriana* forest along an altitudinal gradient in Basu County, SETP. According to the correlation analyses between tree-ring widths and climate variables, the strongest climatic signal in tree-ring growth is mean RH from previous August until the end of July of the year of tree-ring formation, followed by total precipitation over the same seasonal window. In terms of temperatures signals, the correlations were generally weak despite the positive correlations occurring in previous November and current February and April. This suggests a secondary growth limitation resulting from low temperatures that occur prior to the growth season (Fig. 4), possibly due to cold stress or short growing season. Thus, air dryness outweighs the positive effect of temperature and moisture availability and seems to be the major factor controlling the variation in tree growth at treeline. Drought-sensitive tree growth at treelines has also been observed in southern and central parts of the TP (Liang et al. 2014; Liu et al. 2015; Yang et al. 2013).

Relative humidity, an indicator of atmospheric drought conditions, is strongly associated with global warming because of the exponential relationship between the saturated vapour pressure in the air and air temperature (Ding et al. 2018; Eamus et al. 2013). The increase in atmospheric water demand results in a higher potential to pump moisture out of soils and plants, known as the global-change-type drought *sensu* Eamus et al. (2013). In addition to RH, we calculated the vapour pressure deficit (VPD) based on the instrumental records and found

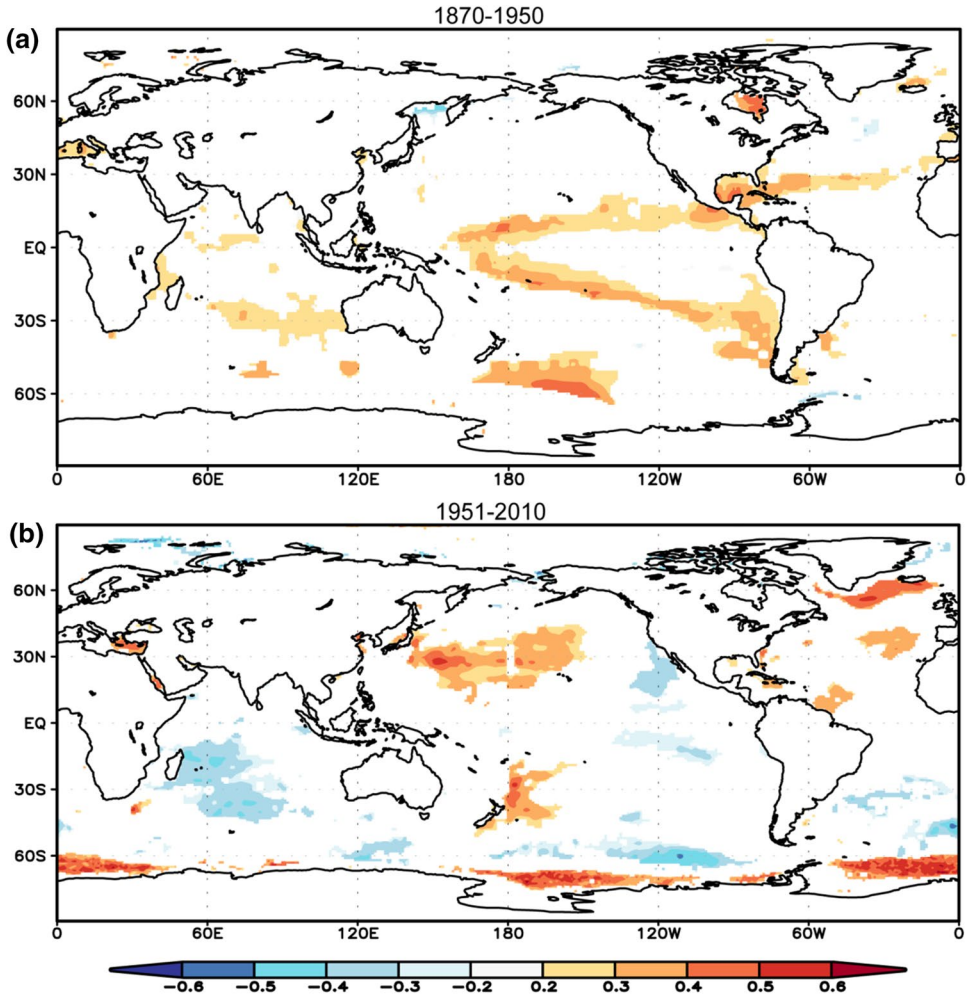

Fig. 7 Correlations between the reconstructed relative humidity and HadlSST1 sea surface temperature (SST) over the periods 1870–1950 (**a**) and 1951–2010 (**b**). The SST was averaged over the same season as the relative humidity reconstruction, i.e., from previous August to current July. Insignificant correlations ($P < 0.10$) were masked out

significant and negative correlations between VPD and tree-ring width variations (Fig. S5). When air humidity is low, trees tend to close their stomata at the cost of reduced carbohydrate assimilation and, subsequently, reduced tree growth (Adams et al. 2009; Eamus et al. 2013; Will et al. 2013). This global-change-type drought is presumed to be exacerbated on the TP given the occurrence of above-average warming (Imtiaz et al. 2013; Xu et al. 2018).

Significant correlations were also found between the total annual precipitation from previous August to current July and tree-ring width (Fig. 4). These results indicate the importance of annual precipitation for tree growth (Fig. 4). According to the climate records, the study area receives less than 300 mm precipitation per year, representing the dry pole of the Tibetan Plateau (Xu 2001). Water availability, which is anyway limited because of the low precipitation in this area, is further lost during surface runoff due to steep slopes and shallow soil layers (Xu 2001). The combination of low precipitation, water loss due to steep terrain, and enhanced evapotranspiration have most probably made water the limiting factor for tree growth in the studied forests, regardless of elevation.

4.2 Comparisons with other reconstructions and documents

To further examine the reliability of the RH_{87} reconstruction, independent hydroclimate reconstructions from the study area and surrounding regions were obtained and compared (Fig. 8). These reconstructions include a Palmer Drought Severity Index (PDSI) reconstruction based on tree-ring width data from northern Tibet (Wang et al. 2008), two summer RH-sensitive tree-ring $\delta^{18}O$ records from the southeastern Tibetan Plateau (Wernicke et al. 2017), a SPEI reconstruction based on tree-ring width data from Biru County of the eastern Tibetan Plateau (Nie et al. 2017), and the closest grid point of the spatio-temporal summer PDSI reconstruction from the Monsoon Asia Drought Atlas (MADA) (Cook et al. 2010).

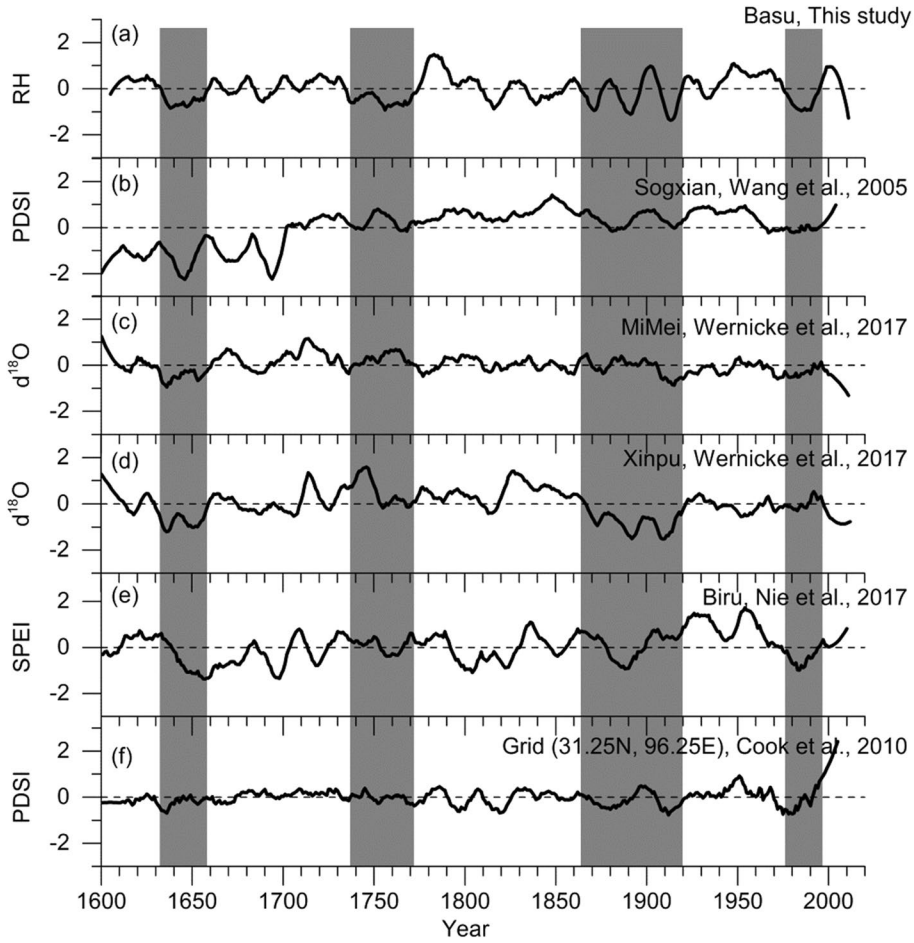

Fig. 8 Comparisons between reconstructed relative humidity of this study (**a**) and independent hydroclimate reconstructions on and around the Tibetan Plateau. **b** Palmer Drought Severity Index (PDSI) reconstruction from Sogxian, north Tibet (Wang et al. 2008); **c, d** Tree-ring cellulose $\delta^{18}O$ records from MiMei and Xinpu (Wernicke et al. 2017); **e** May–June SPEI reconstruction from Biru County/Eastern Tibetan Plateau (Nie et al. 2017); **f** PDSI reconstruction extracted from the gridded dataset MADA (Cook et al. 2010). All of the hydroclimate reconstructions were centred to 0 and rescaled to a standard deviation of 1, and then smoothed using 20-year Sacizky-Golay filters (Savitzky and Golay 1964). Note that the $\delta^{18}O$ series were multiplied by −1 for visual clarity. Note that all of the hydroclimate reconstructions were masked in the sample location map (Fig. 1)

To highlight low-frequency climate signals, all of the compared reconstructions were smoothed using 20-year Savitzky–Golay filters (Savitzky and Golay 1964). Several salient feature periods of our reconstruction were found to correspond to some or all of the other reconstructions (Fig. 8), particularly the two severe dry periods 1907–1919 and 1977–1997, despite different reconstruction targets. The three cold episodes identified in this study form a zigzag-like pattern in the period 1865–1920 (Fig. 5b). Similar pattern was observed in the tree-ring $\delta^{18}O$ variations from the Xinpu site (Wernicke et al. 2017). Another prominent drought period around the 1650s was observed in all the other hydroclimate records but with varying amplitudes and timings. The long-lasting drought period around 1750, however, was generally out of phase with other reconstructions, demonstrating the regional heterogeneity of hydroclimate variations on the TP (Fig. 8).

In addition to the persistent dry or humid periods, our reconstruction discloses a number of extreme years. It is noteworthy that four out of the ten driest years occurred in the twentieth century (i.e., 1914, 1912, 1937, and 1983); these events are all well documented drought years on the TP (Tibet Archive 1990). For instance, the year 1983 was characterized as the driest in the past four centuries (Table 3), possibly resulting from the strongest and most devastating El Niño event on record (Ashok and Yamagata 2009; Caviedes 1984).

4.3 Tree-ring based RH_{87} reconstruction reveals regime shifts of the PDO

The PDO is a leading mode of climate variability that affects precipitation regimes over Asia (D'Arrigo and Wilson 2006; Krishnamurthy and Krishnamurthy 2014) and North America (Mantua and Hare 2002). Although the factors controlling its periodicity and strength remain to be resolved, PDO climate information has been useful for improving annual climate forecasts because of its strong tendency towards multi-year persistence (Mantua and Hare 2002). Hydroclimate variations in Asia (one of the central response regions of the PDO) are in antiphase with the PDO (Yang et al. 2017; Yu et al. 2018; Zhang et al. 2017b). The Walker circulation is closely associated with tropical Pacific SST anomalies (Nakamura et al. 1997; Yu et al. 2018). During positive PDO phases, SSTs tend to be anomalously low in the central North Pacific

and coincident with anomalously warm SSTs in the east (Mantua and Hare 2002). Low pressure over the North Pacific causes enhanced counter-clockwise winds over the North Pacific that strengthens the westward wind over the equatorial Pacific. This leads to a stronger El Niño and colder SSTs in the western Pacific. The transport of moisture from the Bay of Bengal and the South China Sea to the study area is inhibited, leading to anomalous divergence there (Xue et al. 2018; Yang et al. 2017). During negative PDO phases, the distribution for SST anomalies is nearly opposite that during positive PDO phases (Mantua and Hare 2002).

A consistent strong and negative relationship was observed between our reconstruction (RH_{87}) and the PDO at multi-decadal scales during the past four centuries, particularly in the second half of the twentieth century (Fig. 6). According to our reconstruction, the driest episode in the twentieth century started in 1977 and ended in 1997, corresponding to a positive phase of the PDO (Mantua and Hare 2002). This PDO modulation of the decadal variability of RH was observed in another tree-ring based relative humidity reconstruction in northwestern Yunnan, southeast of our study area (Shi et al. 2018). Li et al. (2018) found the PDO to be positively associated with temperatures reconstructed from tree-ring density series from Sygera Mountain on the SETP. This is consistent with the negative association between RH and the PDO observed in our study, which is due to the inherent negative relationship between air temperature and RH (Ding et al. 2018).

The correlation fields between RH_{87} and sea surface temperature (SST) further confirm the distinct teleconnections between the PDO and hydroclimate in our study area (Figs. S8–S10). Beyond the SETP, a continuous response area in southern China was also observed in the correlations between RH_{87} and the spatially gridded vapour pressure in southern but not in northern China (Fig. S11). This is consistent with the "North–South Dipole" pattern of annual precipitation that modulated by the PDO over east China (Yang et al. 2017). It also provides supportive evidence that the western edge of the PDO influence region may extend to the Qamdo Prefecture, SETP.

The teleconnection pattern to the PDO over the SETP was, however, not temporally stable over the past four centuries. In the instrumental record period of PDO, correlations between our RH reconstruction and the PDO series shifted after about 1950 from weak positive to significant negative values, and then to significant positive correlations around 2000 (Fig. 5b). The first turning point of the twentieth century, around 1950, roughly coincided with a well-documented regime shift of the PDO from a warm phase to a cool phase (Nakamura et al. 1997; Newman et al. 2016). The inherent regime shifts of the PDO may therefore have been the trigger for the unstable teleconnection to hydroclimatic variability on the SETP. However, the second turning point of correlations, around 2000, is not well evidenced and the underlying mechanisms are still unknown.

Our reconstruction suggests several shifts in the PDO-RH relationship in the past, and that such behaviour may be expected in the future. Caution should therefore be taken when applying the multi-decadal behaviour of the PDO observed in twentieth century as a basis for anticipating or planning for long-term variability in water resources beyond the immediate future. In particular, we want to draw attention to a unique epoch in the early eighteenth century, when a significant and prolonged inphase relationship was observed between our reconstruction and the PDO. However, the causes of the unstable interactions between the SETP hydroclimate and the multidecadal PDO variability are still unknown. We hope that these results will inspire continued efforts to enhance the mechanistic understanding of the influence of the PDO on hydroclimate on the SETP.

5 Conclusions

This study contributes a well-replicated reconstruction of hydrological-year mean relative humidity (RH_{87}) on the SETP over the past four centuries, where air humidity records are still scarce. We found that the twentieth century was characterized by generally more humid conditions, although four of the ten driest years are observed in this century, with 1983 found to be the driest over the past four centuries. Seven out of the ten most humid years were found in the eighteenth century. Our reconstruction reveals that the PDO is the dominant climate driver at multi-decadal scales, but that the relationships are not stable over time. The mechanisms underlying the PDO-climate relationships remain unknown. These results imply that the PDO may be a useful tool for forecasting regional hydroclimatic variations on the SETP. Additional studies are needed to clarify the PDO mechanisms governing hydroclimate on the TP. Such studies will improve our ability to predict future climate changes under different warming scenarios.

Acknowledgements This research was supported by the Natural Science Foundation of China (Grants Nos. 31330015 and 41771060) and the China Scholarship Council (No. 201770490418). The climate data were obtained from the weather information centre of the China Meteorological Administration. We are grateful to the Tibetan Forestry Bureau for permitting field sampling and the field work team for collecting tree-ring samples. We are also grateful to Prof. Qi-Bin Zhang for commenting on the early version of the manuscript and to Erin Gleeson for editing English texts.

Compliance with ethical standards

Conflict of interest The authors have declared no conflicts of interest for this article.

References

Adams HD et al (2009) Temperature sensitivity of drought-induced tree mortality portends increased regional die-off under global-change-type drought. Proc Nal Acad Sci 106:7063–7066. https://doi.org/10.1073/pnas.0901438106

Allen RG, Pereira LS, Raes D, Smith M (1998) Crop evapotranspiration—guidelines for computing crop water requirements. Food and Agriculture Organization of the United Nations. Rome, Italy **(ISBN 92-5-104219-5)**

Anchukaitis KJ, Buckley BM, Cook ER, Cook BI, D'Arrigo RD, Ammann CM (2010) Influence of volcanic eruptions on the climate of the Asian monsoon region. Geophys Res Lett. https://doi.org/10.1029/2010GL044843

Ashok K, Yamagata T (2009) The El Niño with a difference. Nature 461:481. https://doi.org/10.1038/461481a

Beguería S, Vicente-Serrano SM (2017) SPEI: calculation of the standardised precipitation-evapotranspiration index R package version, vol 17. https://CRAN.R-project.org/package=SPEI. Accessed 26 June 2018

Biondi F, Qeadan F (2008) Inequality in paleorecords. Ecology 89:1056–1067. https://doi.org/10.1890/07-0783.1

Bordi I, Sutera A (2007) Drought monitoring and forecasting at large scale. In: Rossi G, Vega T, Bonaccorso B (eds) Methods and tools for drought analysis and management. Springer, Dordrecht, pp 3–27. https://doi.org/10.1007/978-1-4020-5924-7_1

Bräuning A, Mantwill B (2004) Summer temperature and summer monsoon history on the Tibetan plateau during the last 400 years recorded by tree rings. Geophys Res Lett 31:L24205. https://doi.org/10.1029/2004gl020793

Cai Y et al (2015) Variability of stalagmite-inferred Indian monsoon precipitation over the past 252,000 y. Proc Natl Acad Sci 112:2954–2959. https://doi.org/10.1073/pnas.1424035112

Caviedes CN (1984) El Nino 1982-83. Geogr Rev 74:267–290. https://doi.org/10.2307/214939

Chen N, Jayaprakash C, Yu K, Guttal V (2018) Rising variability, not slowing down, as a leading indicator of a stochastically driven abrupt transition in a dryland ecosystem. Am Nat 191:E1–E14. https://doi.org/10.1086/694821

Chou C, Neelin JD, Chen C-A, Tu J-Y (2009) Evaluating the "Rich-Get-Richer" mechanism in tropical precipitation change under global warming. J Clim 22:1982–2005. https://doi.org/10.1175/2008jcli2471.1

Cook ER, Kairiukstis LA (1990) Methods of dendrochronology: applications in the environmental sciences. Kluwer Academic Press, Dordrecht

Cook ER, Anchukaitis KJ, Buckley BM, D'Arrigo RD, Jacoby GC, Wright WE (2010) Asian monsoon failure and megadrought during the last millennium. Science 328:486–489. https://doi.org/10.1126/science.1185188

D'Arrigo R, Wilson R (2006) On the Asian expression of the PDO. Int J Climatol 26:1607–1617. https://doi.org/10.1002/joc.1326

Ding J et al (2018) Increasingly important role of atmospheric aridity on Tibetan Alpine grasslands. Geophys Res Lett 45:2852–2859. https://doi.org/10.1002/2017GL076803

Duan J, Zhang Q-B (2014) A 449 year warm season temperature reconstruction in the southeastern Tibetan Plateau and its relation to solar activity. J Geophys Res Atmos 119:2014JD022422. https://doi.org/10.1002/2014JD022422

Duan J, Li L, Fang Y (2015) Seasonal spatial heterogeneity of warming rates on the Tibetan Plateau over the past 30 years. Sci Rep 5:11725. https://doi.org/10.1038/srep11725

Eamus D, Boulain N, Cleverly J, Breshears DD (2013) Global change-type drought-induced tree mortality: vapor pressure deficit is more important than temperature per se in causing decline in tree health. Ecol Evol 3:2711–2729. https://doi.org/10.1002/ece3.664

Fan ZX, Bräuning A, Cao KF (2008) Tree-ring based drought reconstruction in the central Hengduan Mountains region (China) since A.D. 1655. Int J Climatol. https://doi.org/10.1002/joc.1689

Fang K et al (2009) Reconstructed droughts for the southeastern Tibetan Plateau over the past 568 years and its linkages to the Pacific and Atlantic Ocean climate variability. Clim Dyn. https://doi.org/10.1007/s00382-009-0636-2

Fritts HC (1976) Tree rings and climate. Academic Press, London, UK **(ISBN 0122684508)**

Gou X, Deng Y, Gao L, Chen F, Cook E, Yang M, Zhang F (2014) Millennium tree-ring reconstruction of drought variability in the eastern Qilian Mountains, northwest China. Clim Dyn. https://doi.org/10.1007/s00382-014-2431-y

Grießinger J, Bräuning A, Helle G, Thomas A, Schleser G (2011) Late Holocene Asian summer monsoon variability reflected by d ^{18}O in tree-rings from Tibetan junipers. Geophys Res Lett 38:L03701. https://doi.org/10.1029/2010gl045988

Grießinger J, Bräuning A, Helle G, Hochreuther P, Schleser G (2017) Late Holocene relative humidity history on the southeastern Tibetan plateau inferred from a tree-ring δ18O record: recent decrease and conditions during the last 1500 years. Quatern Int 430:52–59. https://doi.org/10.1016/j.quaint.2016.02.011

Harris I, Jones PD, Osborn TJ, Lister DH (2014) Updated high-resolution grids of monthly climatic observations—the CRU TS3.10 dataset. Int J Climatol 34:623–642. https://doi.org/10.1002/joc.3711

He M, Yang B, Datsenko N (2014) A six hundred-year annual minimum temperature history for the central Tibetan Plateau derived from tree-ring width series. Clim Dynam 43:641–655. https://doi.org/10.1007/s00382-013-1882-x

Holmes RL (1983) Computer-assisted quality control in tree-ring data and measurement. Tree-Ring Bull 43:69–78

Imtiaz R, Eric S, James RM (2013) Amplified warming projections for high altitude regions of the northern hemisphere mid-latitudes from CMIP5 models. Environ Res Lett 8:024040

Körner C, Paulsen J (2004) A world-wide study of high altitude treeline temperatures. J Biogeogr 31:713–732. https://doi.org/10.1111/j.1365-2699.2003.01043.x

Krishnamurthy L, Krishnamurthy V (2014) Influence of PDO on South Asian summer monsoon and monsoon—ENSO relation. Clim Dyn 42:2397–2410. https://doi.org/10.1007/s00382-013-1856-z

Krishnamurthy L, Krishnamurthy V (2016) Teleconnections of Indian monsoon rainfall with AMO and Atlantic tripole. Clim Dyn 46:2269–2285. https://doi.org/10.1007/s00382-015-2701-3

Kullman L (2002) Rapid recent range-margin rise of tree and shrub species in the Swedish Scandes. J Ecol 90:68–77

Kumar KK, Kumar KR, Rakhecha PR (1987) Comparison of Penman and Thornthwaite methods of estimating potential evapotranspiration for Indian conditions. Theor Appl Climatol 38:140–146. https://doi.org/10.1007/BF00868097

Lamsal P, Kumar L, Shabani F, Atreya K (2017) The greening of the Himalayas and Tibetan Plateau under climate change. Glob Planet Change 159:77–92. https://doi.org/10.1016/j.gloplacha.2017.09.010

Li M, Duan J, Wang L, Zhu H (2018) Late summer temperature reconstruction based on tree-ring density for Sygera Mountain, southeastern Tibetan Plateau. Glob Planet Change 163:10–17. https://doi.org/10.1016/j.gloplacha.2018.02.005

Liang EY, Shao XM, Xu Y (2009) Tree-ring evidence of recent abnormal warming on the southeast Tibetan Plateau. Theor Appl Climatol 98:9–18

Liang E, Dawadi B, Pederson N, Eckstein D (2014) Is the growth of birch at the upper timberline in the Himalayas limited by

moisture or by temperature? Ecology 95:2453–2465. https://doi.org/10.1890/13-1904.1
Liang H, Lyu L, Wahab M (2016) A 382-year reconstruction of August mean minimum temperature from tree-ring maximum latewood density on the southeastern Tibetan Plateau, China. Dendrochronologia 37:1–8. https://doi.org/10.1016/j.dendro.2015.11.001
Liu Y et al (2009) Annual temperatures during the last 2485 years in the mid-eastern Tibetan Plateau inferred from tree rings. Sci China Ser D Earth Sci 52:348–359 https://doi.org/10.1007/2Fs11430-009-0025-z
Liu J, Deng X, Lyu L (2015) Relationship of tree growth and climatic factors at treeline of Picea likiangensisvar. balfourianaforest in Basu County, Xizang. Chin J Plant Ecol 39:442–452. https://doi.org/10.17521/cjpe.2015.0043
Liu Z, Yang M, Wan G, Wang X (2017) The spatial and temporal variation of temperature in the Qinghai-Xizang (Tibetan) Plateau during 1971–2015. Atmosphere 8:214. https://doi.org/10.3390/atmos8110214
Lv L-X, Zhang Q-B (2013) Tree-ring based summer minimum temperature reconstruction for the southern edge of the Qinghai-Tibetan Plateau, China. Clim Res 56:91–101. https://doi.org/10.3354/cr01144
MacDonald GM, Case RA (2005) Variations in the Pacific Decadal Oscillation over the past millennium. Geophys Res Lett 32:L08703. https://doi.org/10.1029/2005GL022478
Mantua NJ, Hare SR (2002) The pacific decadal oscillation. J Oceanogr 58:35–44. https://doi.org/10.1023/a:1015820616384
Michaelsen J (1987) Cross-validation in statistical climate forecast models. J Appl Meteorol Climatol 26:1589–1600. https://doi.org/10.1175/1520-0450(1987)026<1589:CVISCF>2.0.CO;2
Mishra AK, Singh VP (2010) A review of drought concepts. J Hydrol 391:202–216. https://doi.org/10.1016/j.jhydrol.2010.07.012
Morrill C, Overpeck JT, Cole JE (2003) A synthesis of abrupt changes in the Asian summer monsoon since the last deglaciation. Holocene 13:465–476. https://doi.org/10.1191/0959683603hl639ft
Nakamura H, Lin G, Yamagata T (1997) Decadal climate variability in the North Pacific during the recent decades. B Am Meteorol Soc 78:2215–2226 https://doi.org/10.1175/1520-0477(1997)078%3C2215:Dcvitn%3E2.0.Co;2
Newman M et al (2016) The Pacific decadal oscillation. Revisit J Clim 29:4399–4427. https://doi.org/10.1175/jcli-d-15-0508.1
Nie C-Y, Zhang Q-B, Lyu L (2017) Millennium-long tree-ring chronology reveals megadroughts on the southeastern Tibetan Plateau. Tree-Ring Res 73:1–10. https://doi.org/10.3959/1536-1098-73.1.1
Novick KA et al (2016) The increasing importance of atmospheric demand for ecosystem water and carbon fluxes. Nat Clim Change 6:1023. https://doi.org/10.1038/nclimate3114
R Core Team (2018) R: a language and environment for statistical computing. R Foundation for Statistical Computing. Vienna, Austria. http://www.R-project.org/.URL. Accessed 6 June 2018
Rodionov SN (2004) A sequential algorithm for testing climate regime shifts. Geophys Res Lett 31:L09204. https://doi.org/10.1029/2004GL019448
Saurer M, Cherubini P, Siegwolf R (2000) Oxygen isotopes in tree rings of Abies alba: the climatic significance of interdecadal variations. J Geophys Res Atmos 105:12461–12470. https://doi.org/10.1029/2000JD900160
Savitzky A, Golay MJE (1964) Smoothing and differentiation of data by simplified least. Sq Proced Anal Chem 36:1627–1639. https://doi.org/10.1021/ac60214a047
Seager R, Vecchi GA (2010) Greenhouse warming and the 21st century hydroclimate of southwestern. N Am Proc Natl Acad Sci 107:21277–21282. https://doi.org/10.1073/pnas.0910856107
Seager R, Hooks A, Williams AP, Cook B, Nakamura J, Henderson N (2015) Climatology, variability, and trends in the U.S. vapor pressure deficit, an important fire-related meteorological quantity. J Appl Meteorol Climatol 54:1121–1141. https://doi.org/10.1175/jamc-d-14-0321.1
Sheppard PR, Tarasov PE, Graumlich LJ, Heussner KU, Wagner M, Osterle H, Thompson LG (2004) Annual precipitation since 515 BC reconstructed from living and fossil juniper growth of northeastern Qinghai Province, China. Clim Dyn 23:869–881. https://doi.org/10.1007/2Fs00382-004-0473-2
Shi C et al (2018) The response of relative humidity to centennial-scale warming over the southeastern Tibetan Plateau inferred from tree-ring width chronologies. Clim Dyn. https://doi.org/10.1007/s00382-018-4107-5
Smith WK, Germino MJ, Johnson DM, Reinhardt K (2009) The altitude of alpine treeline: a bellwether of climate change effects. Bot Rev 75:163–190. https://doi.org/10.1007/s12229-009-9030-3
Thomson DJ (1982) Spectrum estimation and harmonic analysis. Proc IEEE 70:1055–1096. https://doi.org/10.1109/PROC.1982.12433
Tibet Archive (1990) Tibet disasters records: hail, frost and insect disasters (in Chinese). China Tibetology Publishing House, Beijing
Trnka M et al (2018) Priority questions in multidisciplinary drought research. Clim Res 75:241–260. https://doi.org/10.3354/cr01509
Wan G, Yang M, Liu Z, Wang X, Liang X (2017) The precipitation variations in the Qinghai-Xizang (Tibetan) Plateau during 1961–2015. Atmosphere 8:80. https://doi.org/10.3390/atmos8050080
Wang X, Zhang Q-B (2011) Evidence of solar signals in tree rings of Smith fir from Sygera Mountain in southeast Tibet. J Atmos Sol-Terr Phy 73:1959–1966. https://doi.org/10.1016/j.jastp.2011.06.001
Wang X-C, Zhang Q-B, Ma K-P, Xiao S-C (2008) A tree-ring record of 500-year dry-wet changes in northern Tibet, China. Holocene 18:579–588. https://doi.org/10.1177/0959683608089212
Webster PJ, Magafia VO, Palmer TN, Shukla J, Tomas RA, Yanai M, Yasunari T (1998) Monsoons: Processes, predictability, and the prospects for prediction. J Geophys Res Oceans 103:14451–14510. https://doi.org/10.1029/97JC02719
Wernicke J, Grießinger J, Hochreuther P, Bräuning A (2015) Variability of summer humidity during the past 800 years on the eastern Tibetan Plateau inferred from $\delta^{18}O$ of tree-ring cellulose. Clim Past 11:327–337. https://doi.org/10.5194/cp-11-327-2015
Wernicke J, Hochreuther P, Grießinger J, Zhu H, Wang L, Bräuning A (2017) Multi-century humidity reconstructions from the southeastern Tibetan Plateau inferred from tree-ring $\delta^{18}O$. Glob Planet Change 149:26–35. https://doi.org/10.1016/j.gloplacha.2016.12.013
Wigley TML, Briffa KR, Jones PD (1984) On the average value of correlated time series, with applications in dendroclimatology and hydrometeorology. J Clim Appl Meteorol 23:201–213 https://doi.org/10.1175/1520-0450(1984)023%3C0201:OTAVOC%3E2.0.CO;2
Will RE, Wilson SM, Zou CB, Hennessey TC (2013) Increased vapor pressure deficit due to higher temperature leads to greater transpiration and faster mortality during drought for tree seedlings common to the forest–grassland ecotone. New Phytol 200:366–374. https://doi.org/10.1111/nph.12321
Winkler MG, Wang PK (1993) The Late-Quaternary vegetation and climate of China. In: Wright HE (ed) Global climates since the last glacial maximum. University of Minnesota Press, Minneapolis, pp 221–261
Wu Q, Zhang T (2010) Changes in active layer thickness over the Qinghai–Tibetan Plateau from 1995 to 2007. J Geophys Res Atmos. https://doi.org/10.1029/2009JD012974
Xu L-X (2001) Ecology episode of Xi Zang 50 year. National Publishing house, Beijing (in Chinese)
Xu X, Lu C, Shi X, Gao S (2008) World water tower: an atmospheric perspective. Geophys Res Lett. https://doi.org/10.1029/2008GL035867

Xu G et al (2018) Regional drought shifts (1710–2010) in East Central Asia and linkages with atmospheric circulation recorded in tree-ring $\delta^{18}O$. Clim Dyn. https://doi.org/10.1007/s00382-018-4215-2

Xue X, Chen W, Chen S, Feng J (2018) PDO modulation of the ENSO impact on the summer South Asian high. Clim Dyn 50:1393–1411. https://doi.org/10.1007/s00382-017-3692-z

Yang B, He M, Melvin TM, Zhao Y, Briffa KR (2013) Climate control on tree growth at the upper and lower treelines: a case study in the Qilian mountains, Tibetan Plateau. PLoS One 8:e69065. https://doi.org/10.1371/journal.pone.0069065

Yang Q, Ma Z, Xu B (2017) Modulation of monthly precipitation patterns over East China by the Pacific Decadal Oscillation. Clim Change 144:405–417. https://doi.org/10.1007/s10584-016-1662-9

Yao T et al (2012) Different glacier status with atmospheric circulations in Tibetan Plateau and surroundings. Nat Clim Change 2:663. https://doi.org/10.1038/nclimate1580

You Q, Min J, Lin H, Pepin N, Sillanpää M, Kang S (2015) Observed climatology and trend in relative humidity in the central and eastern Tibetan Plateau. J Geophys Res Atmos 120:3610–3621. https://doi.org/10.1002/2014JD023031

Yu K, Saha MV, D'Odorico P (2017) The effects of interannual rainfall variability on tree–grass composition along Kalahari Rainfall Gradient. Ecosystems 20:975–988. https://doi.org/10.1007/s10021-016-0086-8

Yu E, King MP, Sobolowski S, Otterå OH, Gao Y (2018) Asian droughts in the last millennium: a search for robust impacts of Pacific Ocean surface temperature variabilities. Clim Dyn 50:4671–4689. https://doi.org/10.1007/s00382-017-3897-1

Zhang Y, Wallace JM, Battisti DS (1997) ENSO-like interdecadal variability: 1900–93. J Clim 10:1004–1020. https://doi.org/10.1029/2000JC900034

Zhang Q-B, Evans MN, Lyu L (2015) Moisture dipole over the Tibetan Plateau during the past five and a half centuries. Nat Commun 6:8062. https://doi.org/10.1038/ncomms9062

Zhang W, Zhou T, Zhang L (2017a) Wetting and greening Tibetan Plateau in early summer in recent decades. J Geophys Res Atmos 122:5808–5822. https://doi.org/10.1002/2017JD026468

Zhang Y, Tian Q, Guillet S, Stoffel M (2017b) 500-yr. precipitation variability in Southern Taihang Mountains, China, and its linkages to ENSO and PDO. Clim Change 144:419–432. https://doi.org/10.1007/s10584-016-1695-0

Zhu H-F, Shao X-M, Yin Z-Y, Xu P, Xu Y, Tian H (2011) August temperature variability in the southeastern Tibetan Plateau since AD 1385 inferred from tree rings. Palaeogeogr Palaeocl 305:84–92. https://doi.org/10.1016/j.palaeo.2011.02.017